Audio Engineering Society
Convention Express Paper

Presented at the 161st Convention
2026 October 30-November 1, Nashville, TN, USA

This Express Paper was selected on the basis of a submitted synopsis that has been peer-reviewed by at least two qualified anonymous reviewers. The complete manuscript was not peer reviewed. This Express Paper has been reproduced from the author's advance manuscript without editing, corrections, or consideration by the Review Board. The AES takes no responsibility for the contents. This paper is available in the AES E-Library (http://www.aes.org/e-lib) all rights reserved. Reproduction of this paper, or any portion thereof, is not permitted without direct permission from the Journal of the Audio Engineering Society.

Loudspeaker Motor Design Using Iron Nitride Magnets

Allan Devantier, Andri Bezzola

Niron Magnetics
650 Taft St NE
Minneapolis, MN 55413

Correspondence should be addressed to Allan Devantier (allan.devantier@nironmagnetics.com)

ABSTRACT

This paper evaluates iron nitride permanent magnets as an alternative magnet material for loudspeaker motor design, with emphasis on magnetic performance, package efficiency, demagnetization margin, and thermal stability. Representative woofer and tweeter motors were modeled using nonlinear finite element simulations and compared against established magnet materials including neodymium-iron-boron, ferrite, aluminum-nickel-cobalt, and samarium cobalt. For the woofer study, equivalent motor geometries were developed to maintain comparable voice-coil flux density and steel saturation while varying magnet dimensions and operating point. The iron nitride motor achieved the target gap flux density while reducing magnet mass by approximately 460 g relative to the ferrite baseline, demonstrating a practical design space between ferrite and rare-earth solutions. In the tweeter study, the iron nitride motor was able to match the neodymium baseline flux density with only a modest increase in magnet thickness. Temperature-dependent simulations showed the principal advantage of iron nitride: a very low reversible thermal coefficient. Across the modeled temperature ranges, iron nitride maintained a nearly constant magnet operating point and less than 1% variation in voice-coil flux density, compared with significant flux loss for ferrite and neodymium. These results indicate that iron nitride magnets can support loudspeaker motors with reduced thermal compression, more stable Bl, and more consistent electrical Q, while reducing reliance on critical rare-earth materials.

1 Introduction

For the loudspeaker transducer engineer, magnet-material selection is fundamentally a motor design optimization problem balancing force factor (Bl), mass, thermal stability, package volume, cost, and long-term flux stability. The permanent magnet itself does not determine sound quality directly; rather, it determines how efficiently a given motor topology can generate and maintain the required gap flux density while remaining linear under voice-coil current, temperature rise, and demagnetizing fields. Modern finite-element-based motor design therefore treats the magnet material as one parameter within the broader magnetic circuit consisting of the magnet, pole pieces, top plate, shorting rings, and gap geometry [1-4].

Neodymium-Iron-Boron (NdFeB) is generally the preferred choice when maximum flux density and Bl must be achieved in the smallest possible volume. The introduction of NdFeB enabled substantially more compact loudspeaker motors than equivalent ferrite designs while maintaining comparable or higher gap flux density. However, NdFeB exhibits larger negative temperature coefficients than competing materials and therefore requires careful thermal design, particularly in high-power transducers where voice-coil temperatures can exceed

200°C locally. While high-temperature grades (e.g., SH, UH, EH) are often specified when thermal demagnetization margins are limited, these grades still have large negative thermal coefficients for remanence and coercive force [5-10].

Ferrite (Ceramic) remains the dominant magnet material in professional and consumer loudspeaker production because it provides the lowest cost per unit of magnetic energy while offering excellent corrosion resistance and good long-term stability. The lower remanence and energy product of ferrite require a substantially larger magnet volume to achieve the same gap flux as NdFeB, resulting in heavier motor structures. Nevertheless, from a system-cost perspective ferrite frequently remains the optimal choice whenever enclosure size and transport weight are secondary considerations. The widespread adoption of ferrite motors in woofers and subwoofers reflects the fact that magnetic performance can often be recovered through larger magnetic circuits and optimized pole geometry at significantly lower material cost. This trade-off has been recognized in loudspeaker engineering literature since the introduction of high-energy strontium-ferrite materials and remains valid in contemporary designs [11-13].

Aluminum-Nickel-Cobalt (AlNiCo) 5 occupies a unique position because of its extremely low reversible temperature coefficient and exceptional thermal stability. While its energy product is modest by modern standards and its coercivity is significantly lower than ferrite, NdFeB, or SmCo, AlNiCo can maintain remarkably stable magnetic flux over wide temperature excursions. For loudspeaker motors, the principal engineering limitation is its susceptibility to demagnetization by opposing magnetic fields generated by the voice coil. As a result, AlNiCo 5 motors generally require geometries with high permeance coefficients and carefully engineered return paths to prevent irreversible flux loss. Despite these constraints, AlNiCo 5 remains attractive for specialty transducers and premium instrument loudspeakers where thermal consistency, historical authenticity, or specific motor behaviors are desired [7, 14].

AlNiCo 8 is often selected when a designer wishes to retain many of the thermal advantages of AlNiCo 5 while obtaining significantly greater coercivity and resistance to demagnetization than AlNiCo 5. Through its higher cobalt content and optimized microstructure, AlNiCo 8 achieves coercivity values approximately two to three times higher than conventional AlNiCo 5, allowing the motor to better tolerate the alternating demagnetizing fields generated by high-current voice coils. As a result, AlNiCo 8 has historically been used in high-output compression drivers, professional transducers, and specialized instrument loudspeakers where the thermal stability of AlNiCo is desired but higher magnetic robustness is required. Although its remanence is lower than that of AlNiCo 5, the improved coercivity permits more aggressive magnetic-circuit designs and reduces the risk of partial demagnetization under overload conditions. From a loudspeaker engineering perspective, AlNiCo 8 can therefore be viewed as a compromise between the very high remanence but low coercivity of AlNiCo 5 and the much higher coercivity of rare-earth materials such as SmCo and NdFeB. It remains attractive in applications where long-term thermal stability, low flux-temperature sensitivity, and resistance to magnetic aging are more important than achieving maximum energy product or minimum motor mass. The use of higher-coercivity AlNiCo 8 grades in loudspeaker motors has been discussed in both the loudspeaker engineering literature and permanent-magnet design literature as a means of overcoming the principal limitation of traditional AlNiCo 5 motor structures - susceptibility to demagnetization by voice-coil reaction fields [15, 16].

Samarium-Cobalt (SmCo) is often viewed as the premium engineering solution when the designer requires a rare earth magnet possessing both high energy density and excellent thermal stability. SmCo can achieve flux levels approaching NdFeB while exhibiting significantly lower temperature sensitivity and markedly better resistance to corrosion and thermal demagnetization. These characteristics make SmCo particularly attractive for compression drivers, aerospace systems, defense applications, and other transducers operating in harsh thermal environments. The main disadvantages are material cost, brittleness, and manufacturing complexity. Consequently, SmCo is rarely selected for cost-sensitive loudspeakers but becomes highly attractive when magnetic stability across a wide operating envelope outweighs cost considerations [17,18].

Iron nitride is a new commercially available material that is well suited for applications in loudspeaker motors. It offers the high remanence of the rare earth magnets and coercivity comparable to a Y30-grade ferrite magnet. Thermally, FeN has excellent

properties: a small negative thermal coefficient of remanence $\alpha(B_r) = -0.04\,\%/^\circ C$ and a positive thermal coefficient of coercivity $\beta(H_{ci}) = +0.08\,\%^\circ C$. In contrast, NdFeB and SmCo magnets both have negative thermal coefficients. This makes FeN's maximum energy product much less temperature dependent than NdFeB and even lower than the already excellent thermal dependence of SmCo. Ferrite magnets also have positive thermal coefficients of coercivity, but the absolute values of both coefficients are almost an order of magnitude higher than those of FeN. In this regard, the temperature stability of FeN is equivalent to that of AlNiCo. Unlike the case of AlNiCo where the designer must compromise between the high remanence but low coercivity of AlNiCo 5 and the higher coercivity but low remanence of AlNiCo 8, FeN offers high remanence, coercivity comparable to that of ferrite, and thermal stability over a wide range of operating temperatures. This means that a modest increase in magnet size can accommodate the use of FeN in applications that currently use rare earth magnets, while simultaneously improving temperature dependence [19, 20].

From a practical transducer-design perspective, the selection criteria can be summarized as follows: NdFeB is chosen when minimizing mass and motor volume is paramount; ferrite when minimizing system cost is a priority; AlNiCo when thermal consistency and legacy motor behavior are desired; and SmCo when high flux density must be maintained under severe thermal or environmental conditions. FeN magnets offer an attractive alternative that combines modest mass increase with thermal consistency and reasonably high coercivity. The optimal material is therefore determined not by magnetic strength alone but by a multidimensional trade study involving gap flux density, Bl requirements, thermal compression, demagnetization margin, package constraints, manufacturing cost, and application environment. This system-level approach is consistent with contemporary loudspeaker motor-design methodologies described in AES literature and modern electromagnetic design practice. [1,3].

2 Modeling With Nonlinear Permanent Magnets

In the following sections we will compare two applications with a selection of magnet grades representing the most commonly used in the loudspeaker industry: NdFeB N35SH, Ferrite Y30, AlNiCo 5, AlNiCo 8 and SmCo 26H along with the novel FeN magnets. Important values for the comparison are Br, the remanent flux density that indicates the residual magnetic induction available after magnetization, i.e. magnetic flux density at H=0; Hc, the normal coercive field required to reduce the magnetic flux density to zero, i.e. the magnetic field strength required to bring magnetic flux density to zero; Hci, the intrinsic coercive field that characterizes resistance to irreversible demagnetization; BHmax, the maximum energy product and a measure of the magnetic energy density available from the material; density, which determines the magnet mass for a given volume; and the temperature coefficients $\alpha(B_r)$ and $\beta(H_{ci})$, which describe the reversible change of remanence and intrinsic coercivity, respectively, with temperature.

In loudspeaker motor design, the normal (demagnetization) B-H curve of the permanent magnet material is a fundamental tool used to dimension the magnetic circuit and establish the operating point of the magnet within the motor assembly. The designer selects the magnet geometry such that the load line - determined by the reluctance of the surrounding magnetic circuit - intersects the B-H curve in a region that provides sufficient flux density in the air gap while maintaining stability against demagnetization. This operating point directly determines the achievable flux density B in the gap and, consequently, the force factor Bl, which governs the electromechanical coupling efficiency of the driver. In practice, however, the magnetic materials and ferromagnetic components (e.g., pole piece and top plate) exhibit strong nonlinear behavior, particularly as they approach saturation. The B-H relationship is therefore not strictly linear, and the effective permeability becomes field-dependent. These nonlinearities lead to spatial and current-dependent variations in magnetic flux, which manifest as nonlinear force factor, inductance, and ultimately distortion mechanisms in the loudspeaker output [1,21-23].

For this reason, incorporating nonlinear B-H curves into finite element method (FEM) simulations is critical for accurate loudspeaker motor design. Linearized models can produce substantial errors in the predicted flux distribution, particularly in regions of high magnetic loading or near saturation, whereas nonlinear FEM formulations that use field-dependent permeability derived from measured B-H data can accurately capture flux modulation, eddy current effects, and harmonic distortion generation. AES

research has shown that nonlinear electromagnetic effects are primary contributors to loudspeaker distortion at higher drive levels, and their correct representation is essential for predicting real-world performance and optimizing motor geometries. Consequently, modern loudspeaker design workflows rely heavily on nonlinear FEM simulations based on accurate B-H characterization to ensure both efficient magnetic circuit utilization and low-distortion acoustic output [24-26].

For the following FEM simulations, the B-H curve data for neodymium magnet is taken from K&J Magnetics' online B-H curve calculator [27], data for Ferrite is taken from the "Magnetic B-H Curves" library in ANSYS ® Electromagnetics Suite [28], and the data for AlNiCo 5, AlNiCo 8 and SmCo 26H is taken from the material library of the FEM software FEMM™ [29]. The data for the FeN magnets were obtained from a measurement of a commercial pilot plant sample certified by a third party.

3 Example Woofer Motor Design

3.1 Baseline Design

We have chosen the woofer motor design used in the "Loudspeaker Driver Tutorial Model" of the COMSOL Multiphysics® software Application Gallery [30, 31] as a baseline for comparing the different magnet materials. A 3D cutaway of the woofer and the axisymmetric cross section of the motor are shown in Figure 1. The associated baseline dimensions are shown in Table 1.

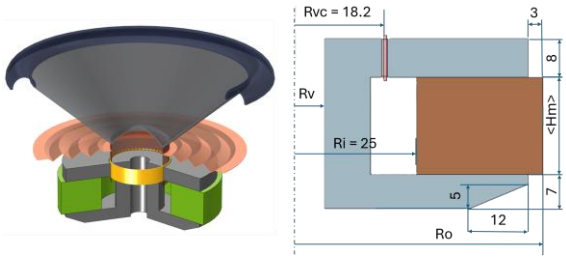


Figure 1: 3D cutaway and 2D axisymmetric cross section of the woofer motor taken from the COMSOL tutorial in [29].

Additional dimensions not shown in Figure 1 are the inner and outer radii of the gap at 17.8 mm and 19 mm respectively, as well as the voice coil width and height of 0.6 mm and 9.4 mm respectively. The baseline dimensions of the magnet consist of the outer radius Ro at 51 mm and height at 20 mm. The magnetization direction is in the axial direction.
We used COMSOL Multiphysics® AC/DC module to simulate the static magnetic circuit and the resulting flux density in the voice coil as well as the magnet operating point.

The steel parts of the motor are modelled with the COMSOL built-in non-linear material called "Soft Iron". The B-H curve for this material is shown in Figure 2, along with curves of 1018 and 1010 cold-rolled steel (CRS) typically used in loudspeaker designs. It is important to highlight that the saturation point is around 1.8 T for the soft iron material.

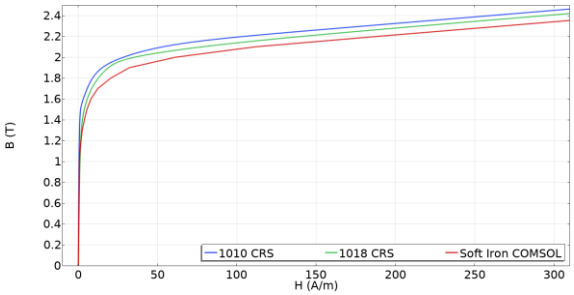


Figure 2: B-H curves for COMSOL's "soft iron" material, 1010 and 1018 cold-rolled steel.

The copper voice coil is modelled using a "Domain Coil" feature of the "Magnetic Fields" interface in the COMSOL Multiphysics® AC/DC Module. Its parameters are given by the number of turns (100), coil wire conductivity ($6 \cdot 10^7$ S/m), and coil wire cross sectional area ($3.5 \cdot 10^{-8}$ m^2). This results in a DC resistance of the voice coil at room temperature of 5.44 Ω.

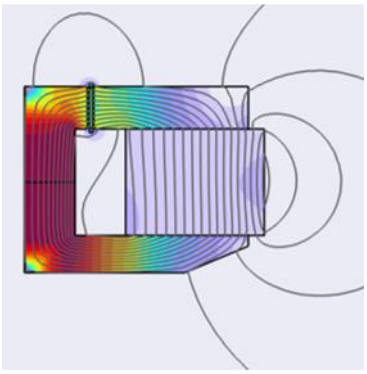


Figure 3: Magnetic field density and flux lines in baseline model with Ferrite Y30 magnet.

The results of the static simulation without any current in the voice coil are shown in Figure 3. It shows a saturated steel pole with an average flux density of 1.85 T in the return pole at the centre height of the magnet. The average radial component of the flux density in the voice coil at rest position, which is centred with the top plate is 0.88 T, resulting in a force factor of $\mathrm{Bl} = 10.1$ N/A.

3.2 Equivalent Motor Designs with Different Magnet Materials

With the given baseline we proceeded to design equivalent loudspeaker motors for the different representative magnet materials described in the introduction.
The following objectives are chosen:

1. Maintain an average radial flux component in the voice coil of 0.875 T to 0.885 T
2. Maintain an average flux through the centre of the return pole piece of 1.84 T to 1.86 T
3. Maintain a comparable operating point of the magnets, while maintaining "reasonable aspect ratios."

The first objective is intended to maintain the motor strength, i.e. Bl value for a given transducer. The second objective is intended to eliminate or at least reduce the nonlinear effects of saturation in the steel pieces. The third objective is intended to make the design of the transducer reasonable, while staying at an operating point where the magnets would not demagnetize from the field generated by the current flowing through the coil, i.e. to "stay away from the knee," as loudspeaker engineers like to say.

To achieve these objectives, we let the following dimensions be design variables:

1. Outer magnet radius (or alternatively magnet annular width)
2. Magnet height
3. Centre vent radius.

Most notably, we maintain the gap dimensions and voice coil dimensions, along with the outer radius of the return pole, top and bottom plate thicknesses, magnet inner radius, and magnet-to-plate overhang.
The resulting design parameter dimensions as well as resulting magnet operating point and mass are given in Table 1. The resulting geometries and saturation plots are shown in Figure 4.

From these results one can see that FeN can be used to replace the baseline ferrite magnet while reducing the magnet mass by about 460 grams. The reduced dimensions will allow the motor to be put into smaller or tighter enclosures, which is a consideration in consumer speakers such as portable speakers or soundbars and lifestyle audio products. The operating point of 4.95 is above the range in the knee where irreversible demagnetization can occur during normal operation.

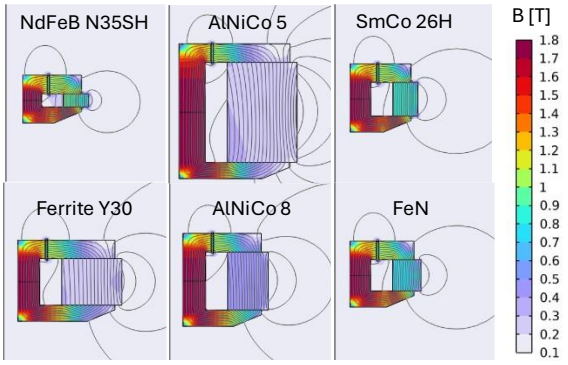


Figure 4: Saturation and flux line plots for motors with different magnet materials.

While AlNiCo 5 and 8 variants can be designed to achieve the target flux density in the voice coil, their operating point is "below" the knee and de-magnetization should be expected with high current flowing through the voice coil. The NdFeB magnet motor is very small and compact, and it could likely benefit from an additional design optimization for the top and bottom plates. It is the lightest solution and while the operating point seems low at 2.56, it is still well in the stable range without any danger of demagnetization.

The SmCo motor design could probably be designed slightly more compact with a lower operating point, but its size is within the range of the FeN magnet. SmCo's mass, however, is significantly higher due to its higher density of $8.3\ \mathrm{g/cm^3}$. For comparison, FeN's density is around $5\ \mathrm{g/cm^3}$.

Table 1: Dimensions, operating point and mass for the equivalent motor designs with different magnet materials.

	Ro [mm]	W [mm]	H [mm]	Rv [mm]	Pc [-]	Mass [g]
NdFeB N35SH	35.7	10.7	5.7	7.2	2.56	88.4
Y30	51	26	20	6	2.89	620.8
AlNiCo 5	55	30	43	4.18	4.37	2,302
AlNiCo 8	42.5	17.5	25	5.6	5.48	658.7
SmCo 26	35.8	10.8	14.5	6.5	5.3	249.8
FeN	37.2	12.2	13.5	6.5	4.95	164.1

3.3 Performance at Various Operating Temperatures

With the designs of the equivalent motors completed, we proceed to investigate the effect of increased (and decreased) operating temperatures on the performance of the motors. Of interest are the values of magnet operating point, flux density in the voice coil, efficiency, and influence on the electrical Q of the motor. In addition to the temperature coefficients for the magnet materials shown in Table 2, the voice coil resistance also changes with temperature. A typical temperature coefficient for resistance in copper is $\alpha_{Cu} = 0.39\%/°\mathrm{C}$. The temperature dependence for the DC resistance of the voice coil can thus be written as:

$$R_e(T) = R_e(20°C) \cdot (1 + \alpha_{Cu}\Delta T). \quad (1)$$

Similarly, for tabulated intrinsic B-H curves of the magnet material, the intrinsic B-H relationship at temperature T can be calculated as:

$$H_i(T) = H_i(20°C) \cdot (1 + \beta(H_{ci})\Delta T), \quad (2)$$

$$B_i(T) = B_i(20°C) \cdot (1 + \alpha(B_r)\Delta T), \quad (3)$$

where the subscript i denotes the intrinsic H and B values respectively.

Values for of $\alpha(B_r)$ and $\beta(H_{ci})$ for the representative magnet grades are given in Table 2.

Table 2: Thermal coefficients of remanence and coercivity for the selected representative magnet grades.

	$\alpha(B_r)$ [%/°C]	$\beta(H_{ci})$ [%/°C]
NdFeB N35SH	-0.12	-0.55
Ferrite Y30	-0.2	0.36
AlNiCo 5	-0.02	0.02
AlNiCo 8	-0.04	0.08
SmCo 26H	-0.03	-0.2
FeN	-0.04	0.08

With the above formulas and the values in Table 2, one can calculate the normal B-H curves at temperature T for simulation. We modelled the above baseline and equivalent alternates at increments of 20 °C between -40 °C and 120 °C.

The average radial component of the flux density in the voice coil at different temperatures is shown in Figure 5. In this plot, the effect of the higher temperature dependence values of $\alpha(B_r)$ and $\beta(H_{ci})$ for neodymium and ferrite magnets becomes very evident. The flux density in the voice coil drops as much as 10.3% for ferrite and 7.1% for neodymium at 120 °C. For the FeN magnet, the variation of the flux density in the voice coil due to temperature is less than 1%. It appears that for AlNiCo magnets, the flux density increases with increasing temperature. This is a sign that the operating point is "below the knee". The flux density in the voice coil for SmCo magnet drops about 1.2% at 120 °C.

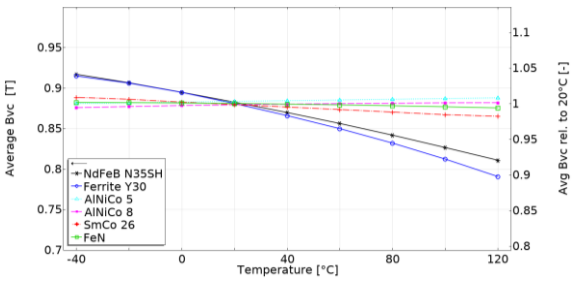


Figure 5: Average radial component of flux density in the voice coil at different temperatures for equivalent motors with different magnet materials.

3.4 Effect of Temperature on Efficiency and Electrical Q-Factor.

The efficiency η of a loudspeaker motor at medium frequencies can be defined as [32, eqn. (6.47)]:

$$\eta = 100\,\frac{B^2 l^2 S_D^2 \rho_0}{\pi R_e M_{MS}^2 c} \propto \frac{B^2}{R_e}, \quad (4)$$

where B is the radial flux density in the voice coil, l is the length of the voice coil wire, S_D is the radiating surface area of the transducer, ρ_0 is the density of air, R_e is the DC resistance of the voice coil, M_{MS} is the mechanical moving mass of the transducer including air load, and c is the speed of sound in air. Of note is that the efficiency is a function of B squared over R_e. Similarly, the electric Q-factor Q_{ES} of a loudspeaker is defined as [32, eqn. (6.30)]:

$$Q_{ES} = \frac{R_e}{2\pi f_S C_{MS} B^2 l^2} \propto \frac{R_e}{B^2}, \quad (5)$$

Where f_S is the mechanical resonance frequency of the transducer and C_{MS} is the mechanical compliance of the transducer suspension.

With the temperature dependence of R_e from equation (1) and the variation of flux density in the voice coil due to temperature from Figure 7, we can now calculate the relative change in mid-range efficiency and relative change in Q_{ES} due to temperature for each equivalent motor. The results are shown in Figure 6. The efficiency and electrical Q-factor in the FeN, AlNiCo, and SmCo motors are clearly dominated by the temperature dependence of the voice coil resistance. At 120 °C, their efficiency is approximately 71% of their efficiency at room temperature. This efficiency drop would result in a drop in SPL of about 1.5 dB.

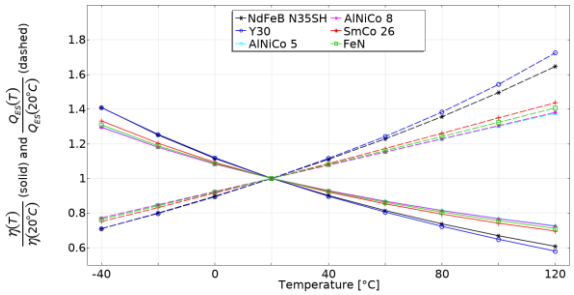


Figure 6: Relative change of efficiency and electrical Q-factor for different operating temperatures in equivalent motor structures with different magnet materials.

Consequently, the electrical Q of those motors at 120 °C is approximately 140% of the electrical Q at room temperature. The motors with neodymium and ferrite magnets see an additional influence of the operating temperature on the magnet material. Their efficiency and electrical Q values at 120 °C are approximately 60% and 170% respectively of their room temperature equivalents. A 60% reduction in efficiency results in a SPL loss of 2.2 dB. That is over 0.7 dB more than for the FeN, AlNiCo, and SmCo magnets.

4 Example Tweeter Motor Design

For the previous example we looked at how a FeN magnet could be used in a woofer with an outer ring magnet. In the following sections, we will investigate the possibility of replacing a neodymium N35SH magnet in a 1-inch tweeter with a FeN magnet.

4.1 Baseline Design

The baseline design is inspired by a FINEmotor tutorial in the AudioExpress journal by Peter Larsen [31,32]. We simplified his design to remove the top bucking magnet and replaced the magnet material with NdFeB N35SH. The magnet dimensions are 24 mm in diameter and 2.5 mm in height. To increase the flux density at the voice coil to about 0.8 T, we had to reduce the vent diameter from 16 mm to 8 mm. The cup extension of 1.25 mm helps with flux symmetry in the gap. The baseline dimensions are shown in Figure 7.

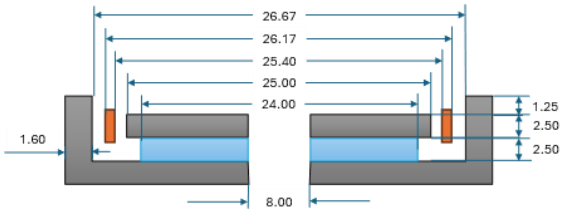


Figure 7: Dimension sketch for the baseline 1-inch tweeter motor.

For this example, we used 1010 cold-rolled steel as the material for the cup and top plate. The height of the coil is 1.91 mm, the number of turns is 23, the bare wire diameter is 0.14 mm, the resistivity of the copper coil material is 1.7 Ωm, resulting in a DC resistance of 3.06 Ω. The resulting flux density and flux line plot for the baseline model is shown in Figure 8 A).

4.2Equivalent Motor Design with an Iron Nitride Magnet

In the next few paragraphs, we will demonstrate how the neodymium magnet of the baseline motor can be substituted by a FeN magnet, resulting in a transducer with equal Bl, but much improved thermal characteristics. We will showcase how a FeN magnet can be used to achieve much higher temperature stability with a minimally larger magnet size.

To achieve a motor outfitted with a FeN magnet that is equivalent to the baseline neodymium magnet motor, we have defined the following targets:

1. Achieve the same radial flux density component in the voice coil
2. Saturate the cup to the same saturation point.

The design parameters that we have varied to achieve these goals are:

1. Height of the magnet
2. Vent diameter
3. Thickness of the cup.

At the nominal operating temperature of 80 °C, the neodymium baseline design achieves a radial flux density of 0.81 T averaged over the voice coil domain. To achieve the same flux density with the FeN magnet, the magnet height needs to grow to 6 mm, the cup thickness needs to be increased from 1.6 mm to 2.0 mm, and the vent diameter can be maintained at 8mm.

The flux density and flux line plots for the equivalent FeN magnet motor design are shown in Figure 8 B).

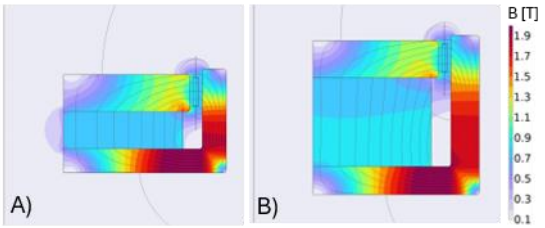


Figure 8: Baseline neodymium tweeter design (A), along with equivalent motor design with a FeN magnet (B).

When plotting the radial component of the flux density at the voice coil over a range of temperatures (see Figure 9), we can again see that the FeN motor is nearly constant, while the NdFeB motor has a relative variation of flux density of +5% at 0 °C to -4% at 120 °C.

5 Conclusions

The simulations presented in this paper indicate that FeN magnets are a viable candidate for loudspeaker motor applications when the motor geometry is designed around the material's specific B-H characteristics. In the woofer example, the FeN motor achieved the target gap flux density and comparable magnetic operating margin while reducing magnet mass by approximately 460 g relative to the ferrite baseline. In the tweeter example, FeN material was shown to achieve equivalent voice-coil flux density to the NdFeB baseline, with the FeN approaching the baseline package constraints closely. These results suggest that FeN can occupy a useful design space between ferrite and rare earth magnet solutions: more compact and lighter than ferrite, less dependent on critical rare earth materials than NdFeB or SmCo, and capable of practical loudspeaker motor performance when the surrounding steel geometry, vent dimensions, and magnet aspect ratio are optimized accordingly.

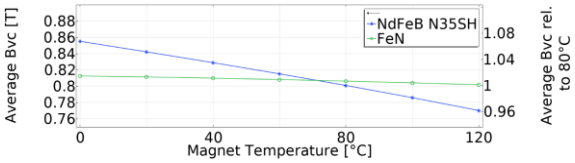


Figure 9: Average radial component of flux density in the voice coil at different temperatures for equivalent tweeter motors with different magnet materials.

The strongest advantage identified for FeN is its thermal stability. Across the modelled temperature ranges, the FeN magnet operating point remained nearly constant, and the resulting voice-coil flux density varied by less than 1%, compared with approximately 7.1% loss for NdFeB and 10.3% loss for ferrite at 120 °C in the woofer motor. Like the AlNiCo and SmCo motors, the FeN motors were thermally limited primarily by the temperature dependence of the copper voice-coil resistance, whereas the NdFeB and ferrite motors suffered additional efficiency loss and Q-factor shift from magnet-temperature sensitivity. In practical loudspeaker terms, this means that FeN offers a path toward motors with reduced thermal compression, more stable Bl, and more consistent electrical Q over the operating range, while avoiding the demagnetization vulnerability observed in the AlNiCo examples. Overall, the analysis supports FeN as a technically capable magnet material for loudspeaker motors, particularly where thermal consistency, reduced rare earth content, and moderate package size are prioritized over the absolute minimum magnet mass achievable with NdFeB.

6 Acknowledgements

The authors would like to thank Niron Magnetics and its team members for supporting this work. Additionally, we would like to extend our gratitude to Doug Button, Jerry Moro, and Tony Morcos for insightful discussions on the use of different magnet types for loudspeaker motors.

References

[1] Dodd, M., "The Transient Magnetic Behaviour of Loudspeaker Motors," in Proc. 111th Conv. Audio Eng. Soc., pp. 5410, New York City, NY (2001 Nov.), https://aes.org/publications/elibrary-page/?id=9819.

[2] Bezzola, A., Brunet P., "Fully Coupled Time Domain Simulations of Loudspeaker Transducer Motors", in Proc. 141st Conv. Audio Eng. Soc., pp. 9599, Los Angeles, CA (2016 Oct.), https://aes.org/publications/elibrary-page/?id=18403.

[3] Eclipse Magnetics, "Magnetic Assemblies for Audio Applications", www.eclipsemagnetics.com/site/assets/files/2172/loudspeakers_assemblies.pdf (accessed July 13, 2026).

[4] Martinek, G., Ruoho, S., Wyss, U., "Magnetic Properties of Permanent Magnets & Measuring Techniques", White-Paper-Measurement-07.23.2021MS2a4.pdf (accessed July 13, 2026).

[5] Arnold Magnetics, "Neodymium-Iron-Boron Magnet Grades", https://www.arnoldmagnetics.com/wp-content/uploads/2017/10/Catalog-151021.pdf (accessed July 13, 2026).

[6] Dura Magnetics, "What is The Effect of Heating Neodymium Magnets: Reversible vs. Irreversible Field Loss", https://www.duramag.com/techtalk/tech-briefs/effects-of-heat-on-neodymium-magnets-reversible-vs-irreversible-field-loss/ (accessed July 13, 2026).

[7] R. Petrie, "Permanent magnets in review," in Proc. of Electrical/Electronics Insulation Conf., pp. 207-210, Chicago, IL (1993), https://doi.org/10.1109/EEIC.1993.631049.

[8] Arnold Magnetics, "Sinetered Neodymium-Iron-Boron Magnets N35SH", https://www.arnoldmagnetics.com/wp-content/uploads/2017/11/N35SH-151021.pdf, (accessed July 13, 2026).

[9] Alliance Magnets, "NdFeB N-35SH", https://allianceorg.com/neodymium-magnets-n35sh.html, (accessed July 13, 2026).

[10] Dura Magnetics, "N35SH", https://www.duramag.com/wp-content/uploads/DuraMag-N35SH.pdf, (accessed July 13, 2026).

[11] Stanford Magnets, "Magnetic Properties of Sintered Ferrite Magnets", (Jun, 2025), https://www.stanfordmagnets.com/magnetic-properties-of-sintered-ferrite-magnets.html, (accessed July 13, 2026).

[12] Magnet Fabriken, "Properties and Magnet Data, Ferrites", https://www.magnetfabriken.com/en/properties-and-magnet-data-ferrites, (accessed July 13, 2026).

[13] A. Cochardt, "Loudspeaker structure with Strontium-ferrite magnets," in IRE Transactions on Audio, vol. AU-10, no. 6, pp. 164-170, (Nov. 1962)

[14] Eclipse Magnetics, "Technical Data Sheet – AlNiCo Magnets", https://www.eclipsemagnetics.com/site/assets/files/22210/eclipsemagnetics_alnico_data_sheet.pdf, (accessed July 13, 2026).

[15] Senz Magnet, "What are the magnetic properties of AlNiCo magnets?", What Are the Magnetic Properties of AlNiCo Magnets? How Do They Differ From Other Magnets (such As Ndfeb Magnet, Ferrite Magnet)?, (accessed July 13, 2026).

[16] Senz Magnet, "Temperature Coefficients and Thermal Stability Analysis of Alnico Magnets", https://www.senzmagnet.com/temperature-

coefficients-and-thermal-stability-analysis-of-alnico-magnets.html, (accessed July 13, 2026).

[17] Allstar Magnetics, "Magnetic Properties of Samarium Cobalt", https://allstarmagnetics.com/wp-content/uploads/2024/09/Samarium-Cobalt-Technical-Data-ASM-09-23-2023.pdf, (accessed July 13, 2026).

[18] Arnold Magnetics, "RECOMA 35E", https://www.arnoldmagnetics.com/wp-content/uploads/2017/10/Arnold_DS_RECOMA35E_FINAL6.pdf, (accessed July 13, 2026).

[19] Johnson, F,. "Iron Nitride Permanent Magnets", submitted to Proc. 161st Audio Eng. Conv., Nashville, TN (Oct. 2026).

[20] Larson, J., "Niron Magnetics: Where We've Been and Where We're Go", submitted to Proc. 161st Audio Eng. Conv., Nashville, TN (Oct. 2026).

[21] Agerkvist, F., Heuchel, F. M., "On the Interdependence of Loudspeaker Motor Nonlinearities", in Proc. 145th Audio Eng. Soc. Conv., pp. 10058, New York City, NY (Oct. 2018), https://aes2.org/publications/elibrary-page/?id=19784.

[22] Svobodnik, A., Shively, R., Chauveau, M.-O., "Multiphysical Simulation Methods for Loudspeakers—Advanced CAE-Based Simulations of Motor Systems" , in Proc. 137th Audio Eng. Conv., pp. 9214, Los Angeles, CA (Oct. 2014). https://aes.org/publications/elibrary-page/?id=17537.

[23] Svobodnik, A., Shively, R., Chauveau, M.-O., Nizzoli, T., "Multiphysical Simulation Methods for Loudspeakers—Nonlinear CAE-Based Simulations" , in Proc. 140th Audio Eng. Conv., pp. 265, Paris, France (June 2016). https://aes.org/publications/elibrary-page/?id=18169.

[24] Fu, X., Yan, S., Zhou, Y., Chen, Z., Xu, X., Ren, Z., "Localized Reluctivity Stabilization of Hysteresis Model for Transient Finite Element Simulation of Ferromagnetic Materials", Eng. 2025, 6(11), pp.289, https://doi.org/10.3390/eng6110289.

[25] Baratelli, M., Munroe, O., "Predicting loudspeaker current distortion with FEA", in Proc. 148th Audio Eng. Conv., pp. 10343, Vienna, Austria (May 2020), https://aes.org/publications/elibrary-page/?id=20760.

[26] Button, D. J., "Design Parameters and Trade-Offs in Large Diameter Transducers", in Proc. 91st Audio Eng. Conv., pp. 3192, New York City, NY (Oct. 1991), https://aes.org/publications/elibrary-page/?id=5524.

[27] K&J Magnetics, "BH Curves Calculator", https://www.kjmagnetics.com/bh-curves.asp, (accessed July 13, 2026).

[28] Ansys® Electromagnetics Suite, Release 2025 R2, Magnetic B-H Curves, Material Data Sample Libraries, ANSYS, Inc. https://www.ansys.com.

[29] D. C. Meeker, Finite Element Method Magnetics, Version 4.2 (21 April 2019 Build), https://www.femm.info.

[30] COMSOL Multiphysics® , "Loudspeaker Driver Tutorial Model", https://www.comsol.com/model/loudspeaker-driver-frequency-domain-analysis-1369, (accessed July 13, 2026).

[31] COMSOL Multiphysics® v. 6.4. www.comsol.com, COMSOL AB, Stockholm, Sweden.

[32] Beranek, L., Mellow, T., Acoustics, Sound Fields and Transducers, (Elsevier, Oxford, UK, 2012). ISBN: 978-0-12-391421-7

[33] Larsen, P., "Loudspeaker Motor Design & Simulation Software", https://loudsoft.com/fine-design-software/, (accessed July 13, 2026).

[34] Larsen, P., "A FINE Circle Speaker Design Tutorial. Part 2 — The Tweeter", Audio Express, (Dec. 2023), https://audioxpress.com/article/a-fine-circle-speaker-design-tutorial-part-2-the-tweeter/, (accessed July 13, 2026).